Wavelet Transforms for Vector Fields Using Omnidirectionally Balanced Multiwavelets

James E. Fowler, *Member, IEEE*, and Li Hua, *Student Member, IEEE*

Abstract— **Vector wavelet transforms for vector-valued fields can be implemented directly from multiwavelets; however, existing multiwavelets offer surprisingly poor performance for transforms in vector-valued signal-processing applications. In this paper, the reason for this performance failure is identified, and a remedy is proposed. A multiwavelet design criterion, omnidirectional balancing, is introduced to extend to vector transforms the balancing philosophy previously proposed for multiwavelet-based scalar-signal expansion. It is shown that the straightforward implementation of a vector wavelet transform, namely the application of a scalar transform to each vector component independently, is a special case of an omnidirectionally balanced vector wavelet transform in which filter-coefficient matrices are constrained to be diagonal. Additionally, a family of symmetric-antisymmetric multiwavelets is designed according to the omnidirectional-balancing criterion. In empirical results for a vector-field compression system, it is observed that the performance of vector wavelet transforms derived from these omnidirectionally-balanced symmetric-antisymmetric multiwavelets is far superior to that of transforms implemented via other multiwavelets and can exceed that of diagonal transforms derived from popular scalar wavelets.**

Keywords— **Vector wavelet transforms, balanced multiwavelets, vector-valued signal processing**

I. Introduction

Wavelet transforms have been some of the most useful signal-processing tools to arise during recent years; however, the overwhelming majority of wavelet literature focuses on the expansion of scalar-valued signals using scalar wavelet systems, i.e., multiresolution analyses consisting of wavelet and scaling functions which are scalar-valued. Yet in many applications, there is a need to process data that is inherently of vector form. For example, fluid flows in oceanography and aerodynamics are usually represented as 2D or 3D vector fields in 2D or 3D space, while images with multiple spectral components can be considered to be 2D fields of multidimensional vectors. These are just two applications out of many for which there is need of a vector wavelet transform (VWT).

The concept of a vector transform has existed for some time [1], and a comprehensive multiresolution-analysis theory for VWTs, which closely parallels theory for scalar-wavelet expansion, was outlined by Xia and Suter [2]. Although Xia and Suter focused on the theoretical infrastructure for VWTs rather than the design of coefficient matrices for vector filter banks, they recognized that multiwavelets present a natural construction for VWTs. Since their introduction [3], multiwavelets have garnered an extraordinary amount of attention from both theorists and engineers, but mostly for the expansion of scalar-valued signals. By expanding a scalar function using several scaling functions and wavelet functions instead of a single pair, multiwavelet-transform systems circumvent certain limitations posed by traditional scalar wavelets, such as the fact that scalar wavelets cannot possess simultaneously orthogonality and linear phase. However, multiwavelets can easily provide expansions for vector-valued signals; in fact, using multiwavelets for vector-valued processing initially appears simpler in that there is no need for scalar-to-vector conversion (which usually involves a polyphase decomposition of the scalar signal and some form of prefiltering [4]).

Given the discussion above, it appears obvious that the large body of existing multiwavelet transforms and filters existing in the literature could be brought to bear directly on the VWT-design problem. However, we demonstrate below that, contrary to expectations, existing multiwavelets perform exceedingly poorly for vector-valued signal-processing applications. As the primary contribution of this paper, we analyze extensively this performance failure and develop a remedy for it. Inspired by the work of Lebrun and Vetterli [5], we find that existing multiwavelets are not suitably "balanced" for vector-valued sources, and adopt a solution we call *omnidirectional balancing* (OB) that greatly improves performance. Employing our OB design criterion, we solve for a family of biorthogonal, symmetric-antisymmetric (SA) multiscaling and multiwavelet functions and corresponding filter banks. Using these OBSA multiwavelets in a VWT, we obtain performance in a simple vector-field compression system far superior to that of existing multiwavelets.

Of course, the most straightforward way to transform vector-valued data is to apply scalar transforms directly by transforming each vector component individually. We show below that such a "product" of multiple scalar transforms is tantamount to an OB VWT with a constrained structure; specifically the filter-coefficient matrices are constrained to be diagonal. Empirical results from our vector-field compression system indicate that our family of biorthogonal OBSA VWTs offers performance that can exceed that of diagonal VWTs based upon the best performing scalar wavelets.

In the following, we provide a brief overview of VWT theory and its relation to multiwavelets in Sec. II and examine the balancing issue for multiwavelets and VWTs in Sec. III. We present the details of the construction of our OBSA multiwavelets in Sec. IV and explore their VWT performance in in Sec. V. Finally, we make some concluding remarks in Sec. VI.

II. Vector Wavelet Transforms

A. Biorthogonal VWT Theory

We now present a brief overview of vector-valued wavelet theory as presented in [2], suitably generalized to the biorthogonal case as employed in [6]. Let $\mathcal{R}$ be the set of real numbers

The authors are with the Department of Electrical & Computer Engineering and the Engineering Research Center, Mississippi State University, Starkville, MS 39762 USA.

This work was funded in part by the National Science Foundation under the Large Data and Scientifi c Software Visualization Program, Grant No. ACI-9982344.

and $\mathcal{Z}$ be the set of integers. The real *matrix-valued signal space* of dimension $N \times N$, $L^2(\mathcal{R}, \mathcal{R}^{N\times N})$, is defined as the set of all *matrix-valued signals*, $\mathbf{f}(t)$, which are $N \times N$ matrices of scalar signals; i.e.,

$$\mathbf{f}(t) = \begin{bmatrix} f_{11}(t) & f_{12}(t) & \dots & f_{1N}(t) \\ f_{21}(t) & f_{22}(t) & \dots & f_{2N}(t) \\ \vdots & \vdots & \vdots & \vdots \\ f_{N1}(t) & f_{N2}(t) & \dots & f_{NN}(t) \end{bmatrix}, \tag{1}$$

where the $f_{ij}(t)$ are scalar-valued functions, $f_{ij}(t) \in L^2(\mathcal{R})$, and $t \in \mathcal{R}$. The integration of matrix-valued function $\mathbf{f}(t)$ is defined as $\int \mathbf{f}(t)\,dt = \left[\int f_{ij}(t)\,dt\right]_{N\times N}$, i.e., the matrix of the integrals of the scalar functions. The inner product of two matrix-valued functions, $\mathbf{f}(t)$ and $\mathbf{g}(t)$, is defined as $\langle \mathbf{f}, \mathbf{g}\rangle = \int_{\mathcal{R}} \mathbf{f}(t)\mathbf{g}^T(t)\,dt$. Note that this is not an inner product in the common sense in which it must be scalar-valued ($\langle \mathbf{f}, \mathbf{g}\rangle$ is an $N \times N$ matrix); however, it can be shown [2] to satisfy properties necessary to be considered to be an inner product for matrix-valued signal spaces. A set of matrix-valued functions, $\Phi_k(t)$, $k \in \mathcal{Z}$, is *orthogonal* to set $\widetilde{\Phi}_l(t)$ if

$$\left\langle \Phi_k(t), \widetilde{\Phi}_l(t) \right\rangle = \delta(k-l)I, \tag{2}$$

where $\delta(n)$ is the Kronecker delta sequence, and I is the $N \times N$ identity matrix. The dual sets $\Phi_k(t)$ and $\widetilde{\Phi}_l(t)$ are called a *biorthogonal basis* if (2) holds, and, for every $\mathbf{f}(t) \in L^2(\mathcal{R}, \mathcal{R}^{N\times N})$, there exists *coefficient matrices*, F_k and $\widetilde{F}_k$, such that $\mathbf{f}(t) = \sum_k F_k \Phi_k(t) = \sum_k \widetilde{F}_k \widetilde{\Phi}_k(t)$. Note that the coefficients in these expansions are $N \times N$ matrices; however, as usual, they can be obtained via inner products, $F_k = \langle \mathbf{f}, \widetilde{\Phi}_k\rangle$, $\widetilde{F}_k = \langle \mathbf{f}, \Phi_k\rangle$.

A biorthogonal multiwavelet multiresolution analysis is driven by two matrix-valued *scaling functions*, $\Phi(t)$ and $\widetilde{\Phi}(t)$, and two matrix-valued *wavelet functions*, $\Psi(t)$ and $\widetilde{\Psi}(t)$, which satisfy matrix-valued *dilation equations*,

$$\Phi(t) = \sqrt{2}\sum_n H_n \Phi(2t-n) \tag{3}$$

$$\widetilde{\Phi}(t) = \sqrt{2}\sum_n \widetilde{H}_n \widetilde{\Phi}(2t-n) \tag{4}$$

$$\Psi(t) = \sqrt{2}\sum_n G_n \Phi(2t-n) \tag{5}$$

$$\widetilde{\Psi}(t) = \sqrt{2}\sum_n \widetilde{G}_n \widetilde{\Phi}(2t-n), \tag{6}$$

and biorthogonality conditions,

$$\left\langle \Phi_{j,k}, \widetilde{\Phi}_{j,l} \right\rangle = \delta(k-l)I \tag{7}$$

$$\left\langle \Phi_{j,k}, \widetilde{\Psi}_{i,l} \right\rangle = \left\langle \widetilde{\Phi}_{j,k}, \Psi_{i,l} \right\rangle = 0 \tag{8}$$

$$\left\langle \Psi_{j,k}, \widetilde{\Psi}_{i,l} \right\rangle = \delta(i-j)\delta(k-l)I, \tag{9}$$

where the coefficient sequences H_n, $\widetilde{H}_n$, G_n, and $\widetilde{G}_n$ are $N \times N$ matrices, and the scales and translates are $\xi_{j,k}(t) = 2^{j/2}\xi(2^j t - k)$, $\xi = \Phi, \widetilde{\Phi}, \Psi, \widetilde{\Psi}$. Translates and scales of scaling functions $\Phi(t)$ and $\widetilde{\Phi}(t)$ and wavelet functions $\Psi(t)$ and $\widetilde{\Psi}(t)$ form a nested sequence of closed subspaces (scaling spaces) and their orthogonal-complement spaces (wavelet spaces) decomposing $L^2(\mathcal{R}, \mathcal{R}^{N\times N})$. Therefore, function $\mathbf{f}(t) \in L^2(\mathcal{R}, \mathcal{R}^{N\times N})$ can be expanded as

$$\mathbf{f}(t) = \sum_k C_{J_0,k}\Phi_{J_0,k}(t) + \sum_{j=J_0}^{\infty}\sum_k D_{j,k}\Psi_{j,k}(t), \tag{10}$$

where J_0 is an arbitrary "starting scale," while scaling coefficients $C_{j,k}$ and wavelet coefficients $D_{j,k}$ are $N \times N$ matrices. Matrix filter-bank equations in the style of Mallat's algorithm [7], the ubiquitous implementation of scalar discrete wavelet transforms, can be derived easily [2].

In most cases, we are actually interested in transforming data consisting of $N \times 1$ vectors rather than $N \times N$ matrices. However, the theory outlined above can still apply. To see this, define signal $\mathbf{f}(t)$ using N identical copies of a given vector source as its N rows, $\mathbf{f}(t) = \begin{bmatrix}\bar{f}(t) & \bar{f}(t) & \cdots & \bar{f}(t)\end{bmatrix}^T$. Then, each row in expansion (10) becomes

$$\bar{f}^T(t) = \sum_k \bar{c}_{j,k}^T \Phi_{J_0,k}(t) + \sum_{j=J_0}^{\infty}\sum_k \bar{d}_{j,k}^T \Psi_{j,k}(t), \tag{11}$$

where each row of the coefficient matrices $C_{j,k}$ and $D_{j,k}$ are identical and equal to $\bar{c}_{j,k}^T$ and $\bar{d}_{j,k}^T$, respectively. In this case, the above theory simplifies since the matrix rows are identical. Since we do not need to calculate identical rows multiple times, the matrix-valued form of Mallat's algorithm (see [2]),

$$\text{Analysis:} \qquad C_{j,k} = \sum_n C_{j+1,n}\widetilde{H}_{n-2k}^T \tag{12}$$

$$D_{j,k} = \sum_n C_{j+1,n}\widetilde{G}_{n-2k}^T \tag{13}$$

$$\text{Synthesis:} \qquad C_{j+1,k} = \sum_n C_{j,n}H_{k-2n} + \sum_n D_{j,n}G_{k-2n} \tag{14}$$

simplifies to

$$\text{Analysis:} \qquad \bar{c}_{j,k} = \sum_n \widetilde{H}_{n-2k}\bar{c}_{j+1,n} \tag{15}$$

$$\bar{d}_{j,k} = \sum_n \widetilde{G}_{n-2k}\bar{c}_{j+1,n} \tag{16}$$

$$\text{Synthesis:} \qquad \bar{c}_{j+1,k} = \sum_n H_{k-2n}^T\bar{c}_{j,n} + \sum_n G_{k-2n}^T\bar{d}_{j,n} \tag{17}$$

where $\bar{c}$ and $\bar{d}$ are scaling and wavelet coefficient vectors of dimension $N \times 1$. We note that an orthonormal VWT is just a special case of a biorthogonal VWT with $\widetilde{H}_n = H_n$, $\widetilde{G}_n = G_n$, $\widetilde{\Phi} = \Phi$, and $\widetilde{\Psi} = \Psi$.

As a consequence of the above definitions, the matrices H_n, $\widetilde{H}_n$, G_n, and $\widetilde{G}_n$ satisfy a matrix version of the perfect-

reconstruction (PR) conditions [6],

$$\sum_n H_n \widetilde{H}^T_{n+2k} = \delta(k) I, \tag{18}$$

$$\sum_n H_n \widetilde{G}^T_{n+2k} = 0, \tag{19}$$

$$\sum_n G_n \widetilde{G}^T_{n+2k} = \delta(k) I, \tag{20}$$

for $k \in \mathcal{Z}$. Finally, we define *two-scale matrix symbols* as

$$H(z) = \frac{1}{\sqrt{2}} \sum_n H_n z^n, \qquad \widetilde{H}(z) = \frac{1}{\sqrt{2}} \sum_n \widetilde{H}_n z^n. \tag{21}$$

B. Diagonal VWTs from Scalar Wavelets

The most straightforward approach to constructing a biorthogonal VWT is to directly apply biorthogonal scalar wavelets, independently, to the individual components of the vector signal. It is fairly straightforward to see that this trivial extension of scalar transformation to the vector case is a special case of a biorthogonal VWT constrained to have scaling and wavelet functions which are diagonal matrix-valued functions. That is, if $\phi(t)$ is the biorthogonal primary scalar scaling function used in the expansion of each vector component (assume we use the same scalar transform for each component), then the corresponding primary vector scaling function is diagonal, $\Phi(t) = \mathrm{diag}\,(\phi(t), \phi(t), \ldots, \phi(t))$. $\Psi(t)$, $\widetilde{\Phi}(t)$, and $\widetilde{\Psi}(t)$ are likewise diagonal. The matrix biorthogonality equations, (7)-(9), hold due to the biorthogonality of scalar functions $\phi(t)$, $\widetilde{\phi}(t)$, $\psi(t)$, and $\widetilde{\psi}(t)$. From the dilation equations, (3)-(6), we see that the H_n, $\widetilde{H}_n$, G_n, and $\widetilde{G}_n$ matrices are also diagonal, and are $H_n = \mathrm{diag}(h_n, \ldots, h_n)$, $\widetilde{H}_n = \mathrm{diag}(\widetilde{h}_n, \ldots, \widetilde{h}_n)$, $G_n = \mathrm{diag}(g_n, \ldots, g_n)$, and $\widetilde{G}_n = \mathrm{diag}(\widetilde{g}_n, \ldots, \widetilde{g}_n)$, where h_n, $\widetilde{h}_n$, g_n, and $\widetilde{g}_n$ are the scalar filters for the biorthogonal transform.

C. Multiwavelet Construction of VWTs

Scalar-valued multiwavelet-based multiresolution analysis consists of scales and translates of a finite number of primary scaling functions, $\phi_1(t)$, $\phi_2(t)$, …, $\phi_N(t)$, dual scaling functions, $\widetilde{\phi}_1(t)$, $\widetilde{\phi}_2(t)$, …, $\widetilde{\phi}_N(t)$, primary wavelet functions, $\psi_1(t)$, $\psi_2(t)$, …, $\psi_N(t)$ and dual wavelet functions, $\widetilde{\psi}_1(t)$, $\widetilde{\psi}_2(t)$, …, $\widetilde{\psi}_N(t)$. In either the scalar case (a special case of multiwavelets wherein $N = 1$), or in the general multiwavelet case (wherein $N > 1$), we expand a single *scalar-valued* function $f(t) \in L^2(\mathcal{R})$ using linear combinations of scales and translates of these scaling and wavelet functions. In contrast, to construct a VWT, we want to expand *vector-valued* functions. However, multiwavelets and VWTs are closely related as was established in [2]. Specifically, in implementing a VWT with multiwavelets, each column of matrix-valued scaling functions $\Phi(t)$ and $\widetilde{\Phi}(t)$ contains a set of multiscaling functions, while each column of the matrix-valued wavelet functions $\Psi(t)$ and $\widetilde{\Psi}(t)$ contains a set of multiwavelet functions. The VWT is implemented as in (15)-(17) directly with H_n, $\widetilde{H}_n$, G_n, and $\widetilde{G}_n$ being the filter coefficient matrices for the multiwavelet system.

III. Multiwavelet Balancing

A. Scalar Balancing

Using biorthogonal multiwavelet filter-coefficient matrices H_n, $\widetilde{H}_n$, G_n, and $\widetilde{G}_n$ in (15)-(17) yields an analysis-synthesis filter-bank pair with perfect reconstruction for use with vector sources. Additionally, if we couple this filter bank with a procedure for "vectorizing" a scalar source, these equations also provide the mechanisms for implementing the forward and inverse discrete multiwavelet transform (DMWT) of a scalar signal; in this case, the multi-input, multi-output filter bank is called a "multifilter" after [8]. The most straightforward way to implement the required vectorization is to separate the scalar signal into its N polyphase components.

It is well known that the mere satisfaction of (18)-(20) is not sufficient to give a DMWT reasonable signal-processing performance for scalar signals. That is, even though (18)-(20) provide perfect reconstruction, the distortions normally introduced by signal-processing operations between analysis and synthesis steps of the multifilter can have dramatically detrimental results.

For example, consider a simple compression system for scalar signals that consists of merely the application of one scale of DMWT analysis, the zeroing of the high-pass or "detail" coefficients ($\bar{d}_{j,k}$ in (16)), and one scale of DMWT synthesis. Suppose this compression system uses the Geronimo-Hardin-Massopust (GHM) multiwavelets [3], which are orthogonal and have $N = 2$. Further suppose we employ a polyphase vectorization which assembles a vector source by placing even samples from the scalar source into the first vector component and odd samples into the second component. If the scalar signal input to the system is the constant signal $[\ldots, 1, 1, 1, 1, 1, 1, \ldots]$, we would expect that the system would reproduce this signal exactly, since our intuition holds that a constant signal would pass perfectly through the "lowpass" branch of the multifilter, and, since we are discarding only highpass coefficients, no change should result. This is, however, not the case. In reality, the output of the system is $[\ldots, 1, \sqrt{2}, 1, \sqrt{2}, 1, \sqrt{2}, \ldots]$, as was observed in [5]. That is, an oscillatory distortion of the scalar constant signal occurs due to the suppression of the detail coefficients from the multifilter. For many other multiwavelets, a similar effect occurs, although the exact values of the oscillations depend on the multiwavelet used. The problem represented by this example is serious as it is likely to lead to significant distortions in any system that modifies coefficients between analysis and synthesis transform steps. This issue is particularly problematic for those processes, notably compression systems, that tend to preserve scaling coefficients at the expense of wavelet coefficients under the assumption that the scaling coefficients provide a "low-resolution" approximation to the original data.

The traditional approach to handling the oscillatory distortions described above is to compensate for them before the forward DMWT is applied. That is, one applies a so-called "prefilter" to the input data before it enters the analysis DMWT filter bank. The net effect, however, is that that the transform itself is changed, usually losing orthogonality or linear phase [5]. An alternative approach was proposed recently [5]. In this technique, it was realized that the root of the problem lies in that the vector $[1, 1]^T$ is not generally an eigenvector of the two-scale matrix

symbols $H(z)$ and $\widetilde{H}(z)$ of (21) when $z = 1$ (corresponding to a zero-frequency, or constant source). To rectify this situation, a similarity transformation was proposed in order to "redesign" the H_n and $\widetilde{H}_n$ matrices such that $[1,1]^T$ is an eigenvector. This approach was called multiwavelet *balancing* [5] due to the fact that it tends to "balance" out the treatment of the vector components by the filter bank.

Specifically, in our formulation of analysis and synthesis, (15)-(17), the conditions imposed by scalar balancing are that we want a constant scalar signal to pass through the lowpass analysis filter unchanged (up to a constant gain); that is, regarding (15), we want $\sum_n \widetilde{H}_n[1,1]^T = \sqrt{2}[1,1]^T$. From the definitions of (21), we have directly that $[1,1]^T$ is a right eigenvector of $\widetilde{H}(z)$ for $z = 1$; that is,

$$\widetilde{H}(1)\begin{bmatrix}1\\1\end{bmatrix} = \begin{bmatrix}1\\1\end{bmatrix}. \tag{22}$$

Additionally, we want a constant signal to pass through the synthesis filter (17) unchanged up to a gain; i.e., $\sum_n H^T_{k-2n}\sqrt{2}[1,1]^T = [1,1]^T$, $\forall k$. Thus, we have that $\sum_n H^T_{2n}\sqrt{2}[1,1]^T = \sum_n H^T_{2n+1}\sqrt{2}[1,1]^T = [1,1]^T$, or equivalently, $\sum_n H^T_n\sqrt{2}[1,1]^T = 2[1,1]^T$. Consequently, we have that $[1,1]$ is a left eigenvector of $H(z)$ when $z = 1$; i.e.,

$$\begin{bmatrix}1 & 1\end{bmatrix} H(1) = \begin{bmatrix}1 & 1\end{bmatrix}. \tag{23}$$

We note that in the original development of [5], only orthonormal multiwavelets were considered, in which case $\widetilde{H}(z) = H(z)$, and (22) and (23) become conditions on the left and right eigenvectors of $H(1)$.

Initially, it may appear that the balancing issue described above applies only to the situation in which a scalar source is processed by first vectorizing it and then applying a DMWT, since it is in the polyphase nature of the vectorization that the oscillations arise. However, as we will see in the next section, purely vector transforms, in which the input data is originally in vector form so that no vectorization is needed, are not immune to this effect. In fact, we will see that a new kind of balancing is needed to rectify the problem, and, in its absence, using multiwavelets for VWTs produces surprisingly poor results for compression.

B. Omnidirectional Balancing

The vector analogue of a constant scalar source is a vector field in which each vector is the same, i.e., $\bar{f}(t) = \begin{bmatrix}a & b\end{bmatrix}^T$, $\forall t$. Define the *orientation* of the constant vector field as $\theta = \tan^{-1}\frac{b}{a}$. From the previous discussion, we would expect some vector other than $\begin{bmatrix}a & b\end{bmatrix}^T$ to be output from the "lowpass" branch of the multifilter, unless $\begin{bmatrix}a & b\end{bmatrix}$ and $\begin{bmatrix}a & b\end{bmatrix}^T$ happen to be a left eigenvector of $H(1)$ and a right eigenvector of $\widetilde{H}(1)$, respectively—but we could apply the scalar balancing to ensure that this is the case. However, doing so would mean that the resulting multiwavelet is "balanced" only for the specific constant source at hand. That is, if we had another constant vector source at a different orientation θ', $\theta' \neq \theta$, the multiwavelet would no longer be balanced for this source. The difference between balancing for vector data and balancing for scalar data is that there is only one constant scalar source to within a gain factor, but infinitely many constant vector sources, all with different orientation angles. This vector balancing problem is exacerbated when the data source is not constant.

Figs. 2 and 3 illustrate the vector balancing problem for the real vector-valued data given in Fig. 1. For Figs. 2 and 3, we perform a 3-scale VWT implemented via a multiwavelet, discard all the wavelet coefficients, and reconstruct using the inverse VWT on just the baseband subband. We implement the 2D VWT in the usual separable fashion—a 1D VWT is taken along each row of vectors and then along each column, yielding three subbands of wavelet coefficients and one baseband of scaling coefficients, repeating then on the baseband. We see that, regardless of whether we use a non-balanced (Fig. 2) or balanced (Fig. 3) multiwavelet for our VWT, we get extremely poor results for our compressor. Specifically, the baseband does *not* consist of a low-resolution approximation of the original data as we are led to expect from scalar multiresolution analysis. We have observed similarly poor results for every multiwavelet we have found in the literature.[1] Since real-world signal-processing algorithms often discard or otherwise modify wavelet coefficients, the practical implications of the vector balancing problem are clear.

To solve the vector balancing problem so as to construct VWTs which are resilient to data loss amongst wavelet coefficients, we propose the following constraint to the VWT-design process. Realizing that the multiwavelet used for the VWT needs to be balanced for *all* vectors lying on the unit circle, we propose a new type of "balancing" that is insensitive to the orientation angle of the vector data so that constant vector sources, regardless of orientation, are reproduced by the "lowpass" branch of the multifilter. Specifically, in terms of (22) and (23), what is required is that all unit vectors are right eigenvectors of $\widetilde{H}(z)$ and left eigenvectors of $H(z)$ when $z = 1$. Such is the case when

$$H(1) = \widetilde{H}(1) = I, \tag{24}$$

where I is the $N \times N$ identity matrix. We call the imposition of (24) *omnidirectional balancing* (OB) as it "balances" the multiwavelet for all orientations in a manner similar to the balancing proposed in [5] for a single direction.

It is well known that, if h_n and $\widetilde{h}_n$ are the scaling filters for a scalar biorthogonal wavelet system, then

$$\sum_n h_n = \sum_n \widetilde{h}_n = \sqrt{2}. \tag{25}$$

The diagonal VWT discussed earlier in Sec. II-B having $H_n = \mathrm{diag}(h_n, \ldots, h_n)$ and $\widetilde{H}_n = \mathrm{diag}(\widetilde{h}_n, \ldots, \widetilde{h}_n)$ thus clearly satisfies (24). Diagonal VWTs constructed from any set of scalar biorthogonal wavelets are thereby OB.

IV. Construction of OBSA Multiwavelet Filters

To construct the primary and dual multiscaling functions for our OBSA VWT, we impose the following set of equations: the

[1] Specifically, we have investigated the multiwavelets appearing in [3, 5, 9–12], and only the multiwavelet based on the complex Daubechies filters of [5] does not suffer from poor performance due to the balancing issue. However, the cascade algorithm for this latter multiwavelet does not converge, so its performance is not competitive either.

PR condition (18), the OB condition (24), and the SA condition [6, 13],

$$H_n = SH_{K_u+K_l-n}S, \qquad \widetilde{H}_n = S\widetilde{H}_{\widetilde{K}_u+\widetilde{K}_l-n}S, \tag{26}$$

where $[K_l, K_u]$ and $[\widetilde{K}_l, \widetilde{K}_u]$ are the intervals of support of the FIR filters H_n and $\widetilde{H}_n$, respectively, and $S = \mathrm{diag}(1, -1, \ldots, (-1)^N)$. We occupy as many remaining degrees of freedom as possible by placing zeros at $z = -1$, corresponding to the technique of vanishing moments widely employed in scalar wavelet design. Specifically, to obtain p zeros at $z = -1$, we have

$$\frac{d^k}{dz^k} H(z) \,\big|_{z=-1} = 0, \tag{27}$$

for $k = 0, 1, \ldots, p$.

After application of the above design steps, there are usually several remaining degrees of freedom, and additional design criteria are necessary to fully determine a solution. In [6], a filter-optimization technique is proposed to occupy degrees of freedom in biorthogonal multiwavelet design. This approach calls for the minimization of the deviation of the magnitude response of the equivalent scalar filter from the ideal, or "brick-wall," scalar lowpass filter. However, the motivation in [6] is to design "good" multifilters for scalar signals; hence, this criterion is not entirely suitable for vector-valued signals. Since it is unclear how to define an ideal vector lowpass filter, we adapt the scalar approach of [6] to our vector design needs as follows.

The technique of [6] is to make the equivalent scalar magnitude response approach that of the ideal lowpass filter by minimizing the objective function E_{lp},

$$\begin{aligned} E_{lp} = {} & \alpha \int_0^{\omega_1} (1 - |H(\omega)|)^2 d\omega + (1-\alpha) \int_{\omega_1}^{\pi} |H(\omega)|^2 d\omega \\ & + \alpha \int_0^{\omega_1} (1 - |\widetilde{H}(\omega)|)^2 d\omega + (1-\alpha) \int_{\omega_1}^{\pi} |\widetilde{H}(\omega)|^2 d\omega, \end{aligned} \tag{28}$$

where α is a weighting parameter, and ω_1 denotes the passband of the ideal lowpass filter. In [6], $|H(\omega)|$ and $|\widetilde{H}(\omega)|$ are the magnitude responses of the equivalent scalar filters. For our vector design problem, we use

$$H(\omega) = \frac{1}{\sqrt{2}} \sum_n H_n e^{jn\omega}, \tag{29}$$

while a variety of definitions exist for the matrix norm. It is unclear which matrix norm is best from a theoretical perspective; however, our empirical observations indicate that all perform equally well. We thus define the matrix norm of $H(\omega) = \big[H_{i,j}(\omega)\big]_{N\times N}$ as

$$|H(\omega)| = \frac{1}{\sqrt{2}} \left(\sum_{i=1}^{N} \sum_{j=1}^{N} \big|H_{i,j}(\omega)\big|^2 \right)^{1/2}, \tag{30}$$

with the division by $\sqrt{2}$ included so as to normalize the DC gain to 1, since our OB condition gives $H(\omega)|_{\omega=0} = I$. Definitions similar to (29) and (30) are used for $|\widetilde{H}(\omega)|$.

For the multiwavelets, we impose biorthogonality between the multiwavelet and multiscaling functions (19), biorthogonality of the dual multiwavelets (20), and a SA condition similar to (26). Similar to (28), we occupy any remaining the degrees of freedom by minimizing a highpass objective function,

$$\begin{aligned} E_{hp} = {} & \alpha \int_0^{\omega_2} |G(\omega)|^2 d\omega + (1-\alpha) \int_{\omega_2}^{\pi} (1 - |G(\omega)|)^2 d\omega \\ & + \alpha \int_0^{\omega_2} |\widetilde{G}(\omega)|^2 d\omega + (1-\alpha) \int_{\omega_2}^{\pi} (1 - |\widetilde{G}(\omega)|)^2 d\omega, \end{aligned} \tag{31}$$

with ω_2 denoting the stopband of the ideal highpass filter.

To date, we have attempted solutions for only the case of $N = 2$, as the overwhelming majority of multiwavelet literature focuses on this multiplicity-2 case, and results are easily visualized for 2D vectors. Additionally, we fix $\alpha = \frac{1}{2}$, and $\omega_1 = \omega_2 = \frac{\pi}{2}$. We present a detailed outline of the solution procedure in the appendix. We have constructed biorthogonal OBSA multiwavelets with this procedure for lengths 7-5 and 5-3; we show the scaling and wavelet functions for the OBSA7-5 filters in Figs. 4 and 5. Filter coefficients for both multiwavelets can be found in the appendix.

V. Experimental Results

Figs. 6 and 7 repeat the experiment of Figs. 2 and 3 for two examples of omnidirectionally balanced VWTs, namely, a diagonal VWT derived from the popular 9-7 biorthogonal scalar wavelet (CDF9-7) [14], and a non-diagonal VWT using our OBSA7-5 multiwavelets. As can be seen, in contrast to Figs. 2 and 3, the basebands of OB VWTs do indeed provide a low-resolution approximation to the original data. Additionally, the mean squared error (MSE) between the reconstructed and original vector fields for Figs. 6 and 7 are significantly smaller than those for Figs. 2 and 3.

To investigate the performance of our OBSA VWTs in a real signal-processing application, we built the following vector-field compression system. Three scales of a 2D VWT for 2D vectors is followed by vector quantization (VQ) of scaling and wavelet coefficient vectors. We use the successive approximation VQ (SAVQ) of [15], which is a hybrid of gain-shape VQ [16] and multistage VQ [16]. Finally, we finish with runlength coding of all insignificant vectors (labeled as "zero" during each approximation pass of the SAVQ coder) and arithmetic coding with multiple contexts. In whole, the system, which produces an embedded bitstream, is roughly an extension to vector data of a coder we developed recently for scalar-valued oceanographic imagery [17, 18].

We have compared the performance of VWTs derived from a number of orthogonal and biorthogonal multiwavelets of both the non-balanced [3, 12, 13] and scalar-balanced [5, 10] variety to that of VWTs created from our OBSA multiwavelets. Rate-distortion performance results for the above compression system using the ocean-current data of Fig. 1 are shown in Fig. 8. We see that our OBSA multiwavelets provide VWTs with performance far superior to VWTs derived from other known multiwavelets. Additionally, in Fig. 9, we have compared the compression performance of diagonal VWTs derived from popular

orthonormal [19] and biorthogonal [14] scalar wavelets to that of VWTs created from our OBSA multiwavelets in the above compression system. From Fig. 9, we see that the compression performance of both of our OBSA VWTs is comparable to that of a diagonal VWT derived from the CDF9-7 biorthogonal wavelet [14], long popular for compression applications. We have repeated these experiments for a number of other vector-valued datasets from a variety of other applications. For example, Fig. 11 repeats the experiments for sea-wind data as illustrated in Fig. 10, and Figs. 13 and 15 compare VWT performance on the two optical-flow fields shown in Figs. 12 and 14, respectively. We see that both of our OBSA VWTs offer performance comparable to the diagonal transforms for the sea-winds data, while our OBSA5-3 VWT outperforms the diagonal transforms for both optical-flow datasets. Thus, we conclude that, although the compression performance of our VWTs is somewhat mixed and dependent on the application producing the vector fields, our nondiagonal OBSA VWTs do have the potential to outperform diagonal VWTs based on popular scalar wavelets.

VI. Conclusions

In this paper, we have revealed that nearly all existing multiwavelets perform poorly when used to implement VWTs. To remedy this situation, we have proposed the incorporation of an additional criterion in the multiwavelet-design procedure that results in multiwavelets that are balanced in an omnidirectional sense. Using this criterion, we design a family of multiplicity-2 OBSA multiwavelets that substantially outperforms existing multiwavelets when used for VWTs in a simple compression system for 2D vectors. Additionally, we show that the straightforward approach to transforming vector data, namely the independent application of scalar transforms in a component-wise fashion, is equivalent to an OB VWT with coefficient matrices constrained to be diagonal. In empirical observations, we find that not only does our family of OBSA multiwavelets provide the best compression performance for VWTs derived from known multiwavelets, it also offers performance comparable to or exceeding that of diagonal OB VWTs based on popular scalar wavelets.

In the future, we hope to incorporate into our OBSA design procedure higher-order balancing constraints akin to those developed in [20] for scalar expansion. Specifically, we propose considering samplings of signals of the form $\bar{x}(t) = x(t)\begin{bmatrix}\cos\theta & \sin\theta\end{bmatrix}^T$, where $x(t)$ is some (scalar-valued) polynomial of degree p, and θ is some arbitrary orientation angle, $\theta \in [0, 2\pi]$. In the order-1 omnidirectional balancing case, $p = 0$, $x(t)$ is equal to some scalar constant, and we have the constant vector field we considered in Sec. III-B. For more general order-p omnidirectional balancing, we would want vector-valued polynomial signals of degree $p-1$ and less to be preserved to within a gain factor by both the lowpass analysis and synthesis operations. We anticipate that factorizations of the $H(z)$ and $\widetilde{H}(z)$ matrices may provide additional design constraints in a manner similar to those used in [20], resulting in even greater vector-field compression performance than what we have demonstrated here.

Acknowledgment

The ocean-current data was obtained from D. N. Fox at NRL-SSC; the sea-wind data from the NASA/NOAA sponsored data system Seaflux at JPL through the courtesy of W. T. Liu and W. Tang; and the optical-low data from the Computer Vision Research Group in the Department of Computer Science, University of Otago, New Zealand.

Appendix

To find OBSA filter coefficients, we use a combination of symbolic solution via Matlab's symbolic toolbox and numerical solution via a gradient descent. Full details of the solution procedure can be found in [21].

Step 1: For given filter lengths, we define coefficient matrices with matrix elements as symbolic variables; the SA condition (26) greatly reduces the number of variables.
Step 2: We impose the PR condition (18), the OB condition (24), and the vanishing-moments conditions (27) and use Matlab's symbolic `solve` function to obtain symbolic solutions. Multiple solutions involving undetermined variables and complex numbers are possible. For example, in solving for our biorthogonal OBSA5-3 filters, we eliminate from further consideration all complex-valued solutions as well as solutions that lead to a purely diagonal structure. We are left with several nondiagonal solutions that differ only in a change of sign. Arbitrarily choosing one, we have

$$H_{-2} = \frac{1}{\sqrt{2}}\begin{bmatrix}\frac{1}{8} & \frac{3}{64\gamma}\\ \gamma & \frac{1}{8}\end{bmatrix}, \qquad H_{-1} = \frac{1}{\sqrt{2}}\begin{bmatrix}\frac{1}{2} & \frac{3}{32\gamma}\\ 2\gamma & \frac{1}{2}\end{bmatrix}$$

$$H_0 = \frac{1}{\sqrt{2}}\begin{bmatrix}\frac{3}{4} & 0\\ 0 & \frac{3}{4}\end{bmatrix}, \quad H_1 = SH_{-1}S, \quad H_2 = SH_{-2}S,$$

$$\widetilde{H}_{-1} = \frac{1}{\sqrt{2}}\begin{bmatrix}\frac{1}{2} & 4\gamma\\ \frac{3}{16\gamma} & \frac{1}{2}\end{bmatrix}, \quad \widetilde{H}_0 = \frac{1}{\sqrt{2}}I, \quad \widetilde{H}_1 = S\widetilde{H}_{-1}S. \tag{32}$$

Step 3: We use a gradient descent to numerically find values of undetermined variables so as to locally minimize the ideal-lowpass objective function (28). For our OBSA5-3 solution, we obtain $\gamma = \frac{\sqrt{3}}{8}$.
Step 4: To solve for G_n and $\widetilde{G}_n$ filters, we again use Matlab's symbolic tools. SA conditions similar to (26) reduce the number of variables, and the biorthogonality equations (19), (20) are solved for symbolic solutions. In the case of our OBSA5-3 filter,

we arrive at

$$G_0 = \frac{1}{\sqrt{2}}\begin{bmatrix} \frac{0.10826939409537}{\beta} & \frac{-3}{16\beta} \\ \frac{-3}{16\zeta} & \frac{0.10823695928027}{\zeta} \end{bmatrix}$$

$$G_1 = \frac{1}{\sqrt{2}}\begin{bmatrix} \frac{-0.21653878819074}{\beta} & 0 \\ 0 & \frac{-0.21647391856054}{\zeta} \end{bmatrix},$$

$$\widetilde{G}_{-1} = \frac{1}{\sqrt{2}}\begin{bmatrix} -0.57726378282811\beta & \beta \\ \zeta & -0.57743676850863\zeta \end{bmatrix}$$

$$\widetilde{G}_0 = \frac{1}{\sqrt{2}}\begin{bmatrix} 2.30905513131246\beta & -2\beta \\ -2\zeta & 2.30974707403452\zeta \end{bmatrix}$$

$$\widetilde{G}_1 = \frac{1}{\sqrt{2}}\begin{bmatrix} -3.46358269696868\beta & 0 \\ 0 & -3.46462061105178\zeta \end{bmatrix},$$

$$G_2 = SG_0S, \quad \widetilde{G}_2 = S\widetilde{G}_0S, \quad \widetilde{G}_3 = S\widetilde{G}_{-1}S. \tag{33}$$

Step 5: We use a gradient descent to numerically find values of undetermined variables so as to locally minimize the ideal-highpass objective function (31). For our OBSA5-3 solution, we find $\beta = 0.26713242893612$ and $\zeta = 0.26712267687476$.

Using the above procedure, we also obtained OBSA filters of length $7/5$, with vanishing moments of order $(3, 1)$. In the symbolic solution of step 2, we arrive at

$$H_{-3} = \frac{1}{\sqrt{2}}\begin{bmatrix} \frac{9+32\lambda}{32(32\lambda-1)} & \frac{48\lambda+512\lambda^2+3}{512(32\lambda-1)\xi} \\ \xi & \lambda \end{bmatrix}$$

$$H_{-2} = \frac{1}{\sqrt{2}}\begin{bmatrix} \frac{7+96\lambda}{16(32\lambda-1)} & \frac{48\lambda+512\lambda^2+3}{128(32\lambda-1)\xi} \\ 4\xi & 2\lambda+\frac{1}{8} \end{bmatrix}$$

$$H_{-1} = \frac{1}{\sqrt{2}}\begin{bmatrix} \frac{5(-5+96\lambda)}{32(32\lambda-1)} & \frac{5(48\lambda+512\lambda^2+3)}{512(32\lambda-1)\xi} \\ 5\xi & -\lambda+\frac{1}{2} \end{bmatrix}$$

$$H_0 = \frac{1}{\sqrt{2}}\begin{bmatrix} \frac{5(-3+32\lambda)}{8(32\lambda-1)} & 0 \\ 0 & -4\lambda+\frac{3}{4} \end{bmatrix}$$

$$\widetilde{H}_{-2} = \frac{1}{\sqrt{2}}\begin{bmatrix} 4\lambda & 4\xi \\ \frac{48\lambda+512\lambda^2+3}{128(32\lambda-1)\xi} & \frac{9+32\lambda}{8(32\lambda-1)} \end{bmatrix}$$

$$\widetilde{H}_{-1} = \frac{1}{\sqrt{2}}\begin{bmatrix} \frac{1}{2} & 8\xi \\ \frac{48\lambda+512\lambda^2+3}{64(32\lambda-1)\xi} & \frac{1}{2} \end{bmatrix}$$

$$\widetilde{H}_0 = \frac{1}{\sqrt{2}}\begin{bmatrix} 1-8\lambda & 0 \\ 0 & \frac{96\lambda-13}{4(32\lambda-1)} \end{bmatrix}$$

$$H_1 = SH_{-1}S, \quad H_2 = SH_{-2}S, \quad H_3 = SH_{-3}S,$$
$$\widetilde{H}_1 = S\widetilde{H}_{-1}S, \quad \widetilde{H}_2 = S\widetilde{H}_{-2}S, \tag{34}$$

while in the numerical optimization of step 3, we obtain $\xi = 0.10519112376824$ and $\lambda = 0.13007432508989$. For the high-pass filters, the symbolic solution of step 4 yields

$$G_{-1} = \frac{1}{\sqrt{2}}\begin{bmatrix} \frac{0.05472555812358}{\rho} & \frac{-0.04423654423260}{\rho} \\ \frac{-0.04423654423260}{\tau} & \frac{0.05470324933616}{\tau} \end{bmatrix}$$

$$G_0 = \frac{1}{\sqrt{2}}\begin{bmatrix} \frac{-0.05259066122941}{\rho} & \frac{0.08847308846520}{\rho} \\ \frac{0.08847308846520}{\tau} & \frac{-0.05257176749455}{\tau} \end{bmatrix}$$

$$G_1 = \frac{1}{\sqrt{2}}\begin{bmatrix} \frac{-0.00426979378833}{\rho} & 0 \\ 0 & \frac{-0.00426296368321}{\tau} \end{bmatrix}$$

$$\widetilde{G}_{-2} = \frac{1}{\sqrt{2}}\begin{bmatrix} -1.23660765742734\rho & \rho \\ \tau & -1.23711196416754\tau \end{bmatrix}$$

$$\widetilde{G}_{-1} = \frac{1}{\sqrt{2}}\begin{bmatrix} 3.66163923915863\rho & -4\rho \\ -4\tau & 3.66307495957489\tau \end{bmatrix}$$

$$\widetilde{G}_0 = \frac{1}{\sqrt{2}}\begin{bmatrix} -3.51708803978847\rho & 5\rho \\ 5\tau & -3.51829216079169\tau \end{bmatrix}$$

$$\widetilde{G}_1 = \frac{1}{\sqrt{2}}\begin{bmatrix} 2.18411291611436\rho & 0 \\ 0 & 2.18465833076869\tau \end{bmatrix}$$

$$G_2 = SG_0S, \quad G_3 = SG_{-1}S,$$
$$\widetilde{G}_2 = S\widetilde{G}_0S, \quad \widetilde{G}_3 = S\widetilde{G}_{-1}S, \quad \widetilde{G}_4 = S\widetilde{G}_{-2}S, \tag{35}$$

and the numeric optimization of step 5 gives us $\rho = 0.12552236275346$ and $\tau = 0.12549181109414$.

REFERENCES

[1] W. Li, "On vector transformation," *IEEE Transactions on Signal Processing*, vol. 41, no. 11, pp. 3114–3126, November 1993.

[2] X.-G. Xia and B. W. Suter, "Vector-valued wavelets and vector filter banks," *IEEE Transactions on Signal Processing*, vol. 44, no. 3, pp. 508–518, March 1996.

[3] J. S. Geronimo, D. P. Hardin, and P. R. Massopust, "Fractal functions and wavelet expansions based on several scaling functions," *Journal of Approximation Theory*, vol. 78, no. 3, pp. 373–401, September 1994.

[4] X.-G. Xia, J. S. Geronimo, D. P. Hardin, and B. W. Suter, "Design of prefilters for discrete multiwavelet transforms," *IEEE Transactions on Signal Processing*, vol. 44, no. 1, pp. 25–35, January 1996.

[5] J. Lebrun and M. Vetterli, "Balanced multiwavelets theory and design," *IEEE Transactions on Signal Processing*, vol. 46, no. 4, pp. 1119–1125, April 1998.

[6] H. H. Tan, L.-X. Shen, and J. Y. Tham, "New biorthogonal mulitwavelets for image compression," *Signal Processing*, vol. 79, no. 1, pp. 45–65, November 1999.

[7] S. G. Mallat, "A theory for multiresolution signal decomposition: The wavelet representation," *IEEE Transactions on Pattern Analysis and Machine Intelligence*, vol. 11, no. 7, pp. 674–693, July 1989.

[8] G. Strang and V. Strela, "Short wavelets and matrix dilation equations," *IEEE Transactions on Signal Processing*, vol. 43, no. 1, pp. 108–115, January 1995.

[9] G. M. Davis, V. Strela, and R. Turcajová, "Multiwavelet construction via the lifting scheme," in *Wavelet Analysis and Multiresolution Methods*, T.-X. He, Ed. Marcel Dekker, Inc., New York, 2000.

[10] I. W. Selesnick, "Balanced multiwavelet bases based on symmetric FIR filters," *IEEE Transactions on Signal Processing*, vol. 48, no. 1, pp. 184–191, January 2000.

[11] L. Shen, H. H. Tan, and J. Y. Tham, "Symmetric-antisymmetric orthonormal multiwavelets and related scalar wavelets," *Applied and Computational Harmonic Analysis*, vol. 8, no. 3, pp. 258–279, May 2000.

[12] V. Strela, "A note on construction of biorthogonal multi-scaling functions," in *Wavelets, Multiwavelets, and Their Applications*, A. Aldroubi and E. Lin, Eds., vol. 216 of *Contemporary Mathematics*, pp. 149–157. American Mathematical Society, 1998.

[13] C. K. Chui and J. Lian, "A study of orthonormal multi-wavelets," *Applied Numerical Mathematics*, vol. 20, no. 3, pp. 273–298, March 1996.

[14] A. Cohen, I. Daubechies, and J.-C. Feauveau, "Biorthogonal bases of compactly supported wavelets," *Communications on Pure and Applied Mathematics*, vol. 45, no. 5, pp. 485–560, May 1992.
[15] E. A. B. da Silva, D. G. Sampson, and M. Ghanbari, "Super high definition image coding using wavelet vector quantization," *IEEE Transactions on Circuits and Systems for Video Technology*, vol. 6, no. 4, pp. 399–406, August 1996.
[16] A. Gersho and R. M. Gray, *Vector Quantization and Signal Compression*, Kluwer Academic Publishers, Norwell, MA, 1992.
[17] J. E. Fowler and D. N. Fox, "Embedded wavelet-based coding of three-dimensional oceanographic images with land masses," *IEEE Transactions on Geoscience and Remote Sensing*, vol. 39, no. 2, pp. 284–290, February 2001.
[18] J. E. Fowler and D. N. Fox, "Wavelet-based coding of three-dimensional oceanographic images around land masses," in *Proceedings of the International Conference on Image Processing*, Vancouver, Canada, September 2000, pp. 431–434.
[19] I. Daubechies, "Orthonormal bases of compactly supported wavelets," *Communications on Pure and Applied Mathematics*, vol. 41, pp. 909–996, November 1988.
[20] J. Lebrun and M. Vetterli, "High-order balanced multiwavelets: Theory, factorization, and design," *IEEE Transactions on Signal Processing*, vol. 49, no. 9, pp. 1918–1930, September 2001.
[21] L. Hua and J. E. Fowler, "Technical details on a family of omnidirectionally balanced symmetric-antisymmetric multiwavelets," Tech. Rep. MSSU-COE-ERC-02-08, Engineering Research Center, Mississippi State University, May 2002.
[22] B. K. P. Horn and B. G. Schunck, "Determining optical flow," *Artificial Intelligence*, vol. 16, no. 1-3, pp. 185–203, August 1981.

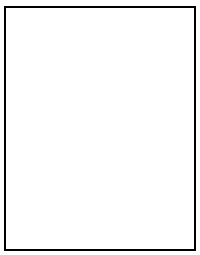

James E. Fowler received the B.S. degree in computer and information science engineering and the M.S. and Ph.D. degrees in electrical engineering in 1990, 1992, and 1996, respectively, all from the Ohio State University. In 1995, he was an intern researcher at AT&T Labs in Holmdel, NJ, and, from January to July of 1997, he held an NSF-sponsored postdoctoral assignment at the Université de Nice-Sophia Antipolis, France. He is currently an assistant professor in the Department of Electrical & Computer Engineering, as well as a researcher in the Engineering Research Center, at Mississippi State University in Starkville, MS. His research interests include image and video coding, data compression, and wavelets.

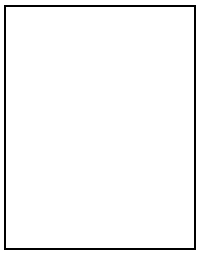

Li Hua received the B.S. and the M.S. degrees in electrical engineering in 1997 and 1999, respectively, from Nanjing University, Nanjing, China. She is currently pursuing the Ph.D. degree in electrical engineering at Mississippi State University. Since 2000, she has been a research assistant in the Engineering Research Center at Mississippi State University, Starkville, MS. Her research interests include image and signal processing, video coding, and wavelets.

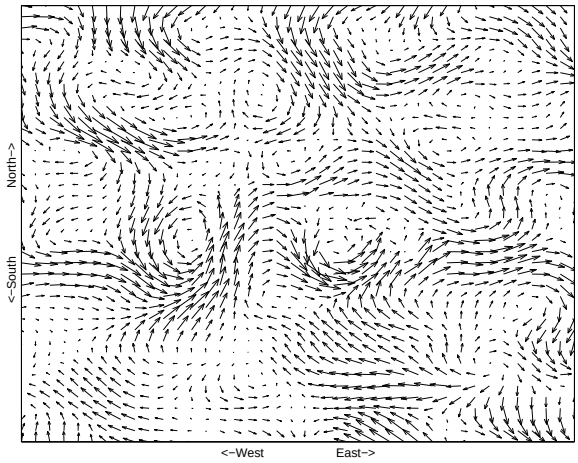

Fig. 1. Original data, a 2D field of 2D vectors representing ocean currents as measured on the surface of the Pacific Ocean.

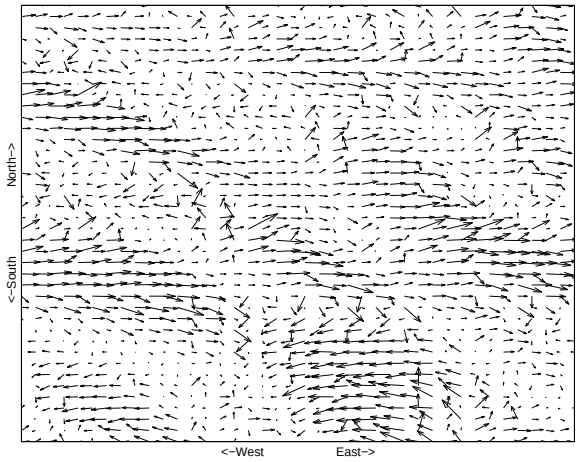

Fig. 2. Reconstruction from the baseband of a VWT implemented with the Chui-Lian length-3 multiwavelet [13], MSE = 0.0334.

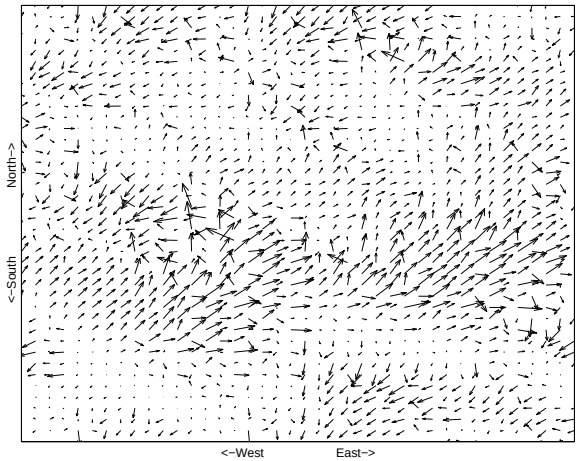

Fig. 3. Reconstruction from the baseband of a VWT implemented with the Lebrun-Vetterli balanced length-3 multiwavelet [5], MSE = 0.0394.

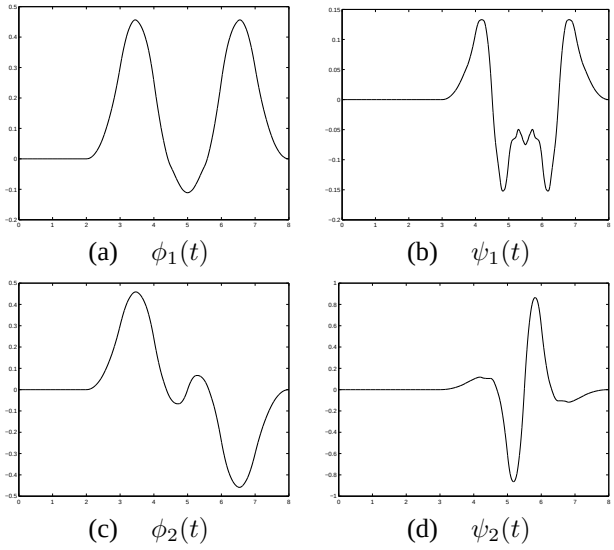

Fig. 4. The primary scaling and wavelet functions of our OBSA7-5 multiwavelets.

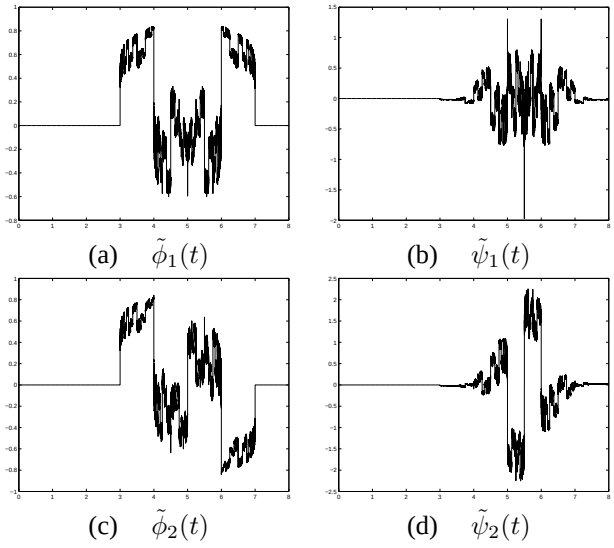

Fig. 5. The dual scaling and wavelet functions of our OBSA7-5 multiwavelets.

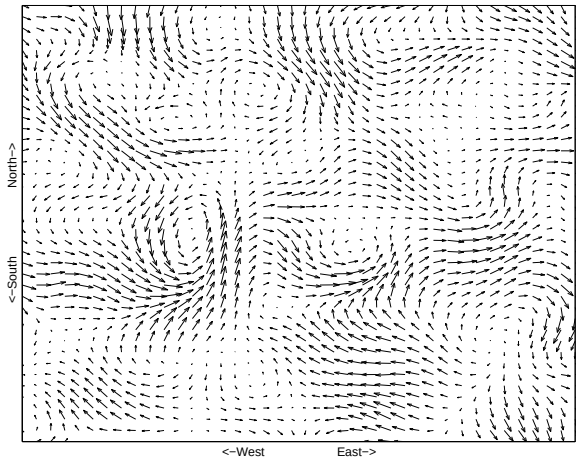

Fig. 6. Reconstruction from the baseband of a diagonal VWT implemented with scalar CDF9-7 biorthogonal wavelets [14], MSE = 0.0076.

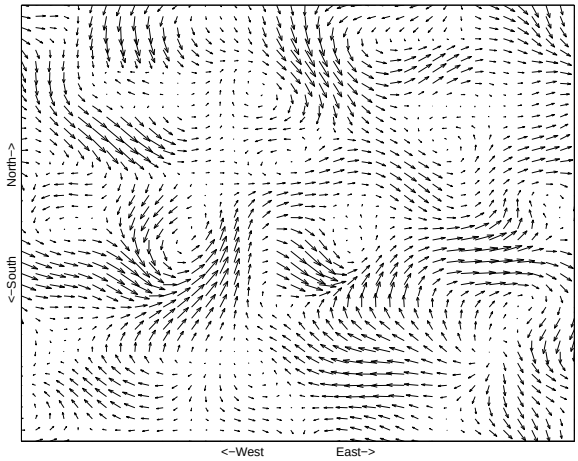

Fig. 7. Reconstruction from the baseband of a VWT implemented with our OBSA7-5 biorthogonal multiwavelets, MSE = 0.0082.

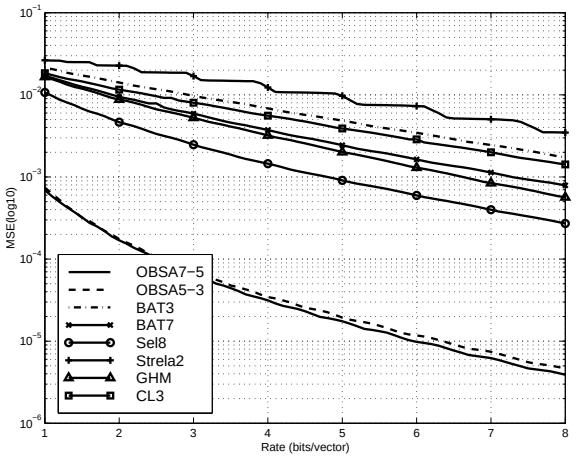

Fig. 8. Compression performance for the ocean-current data of Fig. 1 for VWTs derived from non-balanced multiwavelets (CL3 [13], GHM [3], Strela2 [12]), scalar-balanced multiwavelets (BAT3 [5], BAT7 [5], Sel8 [10]), and our OBSA multiwavelets.

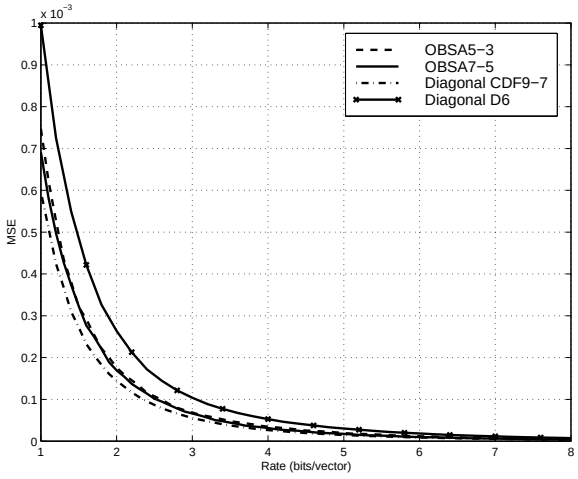

Fig. 9. Compression performance for the ocean-current data of Fig. 1 for VWTs from our OBSA multiwavelets, a diagonal VWT from a scalar orthonormal wavelet (D6 [19]), and a diagonal VWT from a scalar biorthogonal wavelet (CDF9-7 [14]).

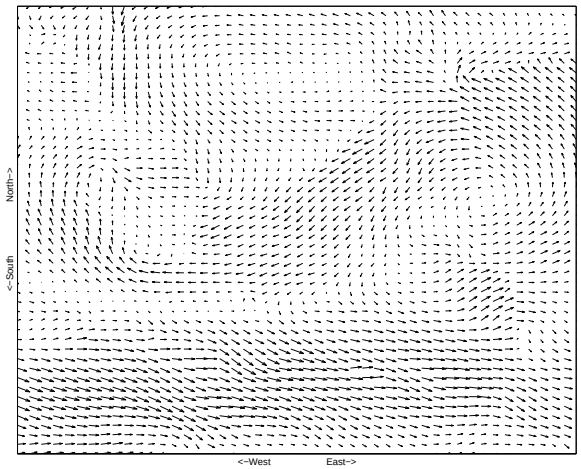

Fig. 10. A 2D field of 2D vectors representing ocean-surface winds derived from scatterometer observations from space.

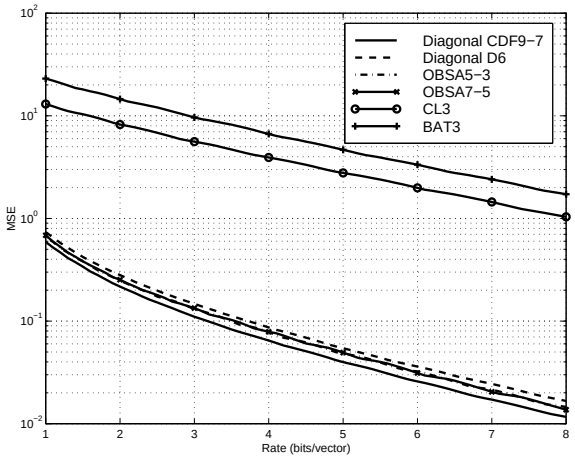

Fig. 11. Compression performance for the sea-wind data of Fig. 10 for VWTs from our OBSA multiwavelets, a diagonal VWT from a scalar orthonormal wavelet (D6 [19]), a diagonal VWT from a scalar biorthogonal wavelet (CDF9-7 [14]), a VWT from a non-balanced multiwavelet (CL3 [13]), and a VWT from a scalar-balanced multiwavelet (BAT3 [5]).

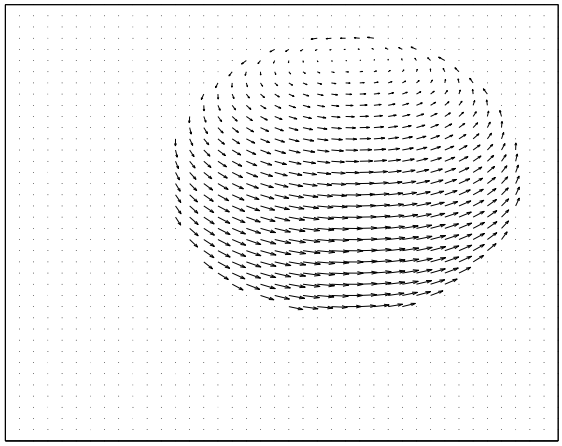

Fig. 12. A 2D field of 2D vectors representing optical flow [22] in a computer-generated rendering of a rotating sphere.

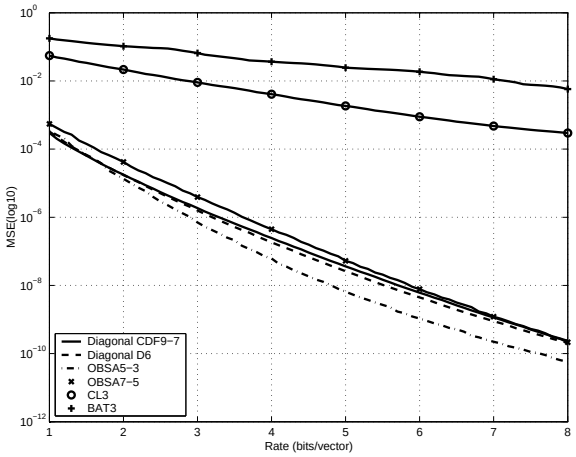

Fig. 13. Compression performance for the optical-flow data of Fig. 12 for the VWTs used in Fig. 11.

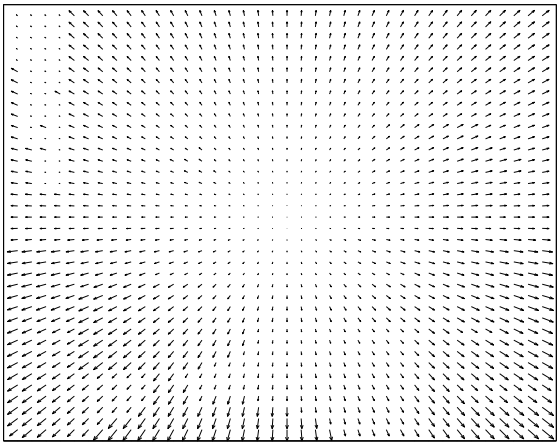

Fig. 14. A 2D field of 2D vectors representing optical flow in a computer-generated rendering of camera zoom in an office.

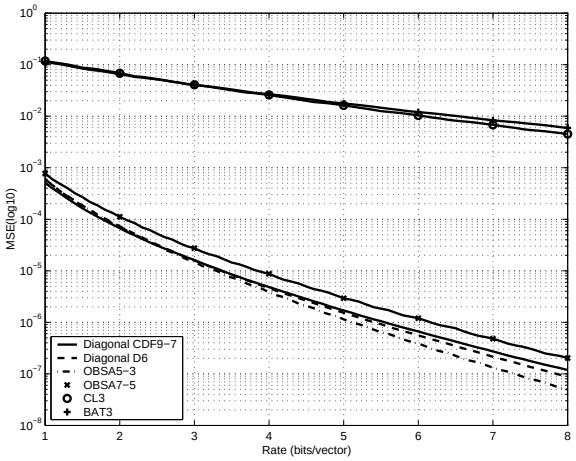

Fig. 15. Compression performance for the optical-flow data of Fig. 14 for the VWTs used in Fig. 11.